



# Graphene oxide in the remediation of norfloxacin from aqueous matrix: simultaneous adsorption and degradation process

Victor Rezende Moreira<sup>1</sup> · Yuri Abner Rocha Lebron<sup>1</sup> · Marielle Mara da Silva<sup>2</sup> · Lucilaine Valéria de Souza Santos<sup>1,2</sup> · Raquel Sampaio Jacob<sup>3</sup> · Cláudia Karina Barbosa de Vasconcelos<sup>2,4</sup> · Marcelo Machado Viana<sup>5</sup> 

Received: 22 April 2020 / Accepted: 8 June 2020 / Published online: 17 June 2020  
© Springer-Verlag GmbH Germany, part of Springer Nature 2020

## Abstract

In the present study, the simultaneous adsorption degradation of norfloxacin (NOR) by graphene oxide from aqueous matrix was verified. Graphene oxide (GO, ~ 8 layers) was prepared using modified Hummers method through the oxidation/exfoliation of expanded graphite. Spectroscopic techniques confirmed the NOR adsorption onto GO surface and the partial antibiotic degradation promoted by hydroxyl radicals derived from GO. Furthermore, the mass spectra after the adsorption-degradation processes showed NOR degradation intermediates that was compared and confirmed by other studies. The nanomaterial showed a removal capacity of  $374.9 \pm 29.8 \text{ mg g}^{-1}$ , observing greater contribution from the NOR in the zwitterionic form and removals up to 94.8%. The intraparticle diffusion process, assessed by Boyd's model and Fick's law, presented a greater contribution in the removal process, reaching the equilibrium 30 min after the beginning. In addition, the temperature increase would disadvantage the process, which was considered thermodynamically viable throughout the evaluated temperature range. Finally, the process was scaled-up in a single stage batch adsorber considering a NOR removal efficiency of 95%. This resulted in mass requirement of 63.6 g of GO in order to treat  $0.5 \text{ m}^3$  of contaminated water. In general, the simultaneous adsorption-degradation process was considered innovative and promising in pharmaceutical compounds remediation.

**Keywords** Adsorption · Emerging contaminants · Nanotechnology · Graphene · Water treatment

Responsible editor: Tito Roberto Cadaval Jr

**Electronic supplementary material** The online version of this article (<https://doi.org/10.1007/s11356-020-09656-6>) contains supplementary material, which is available to authorized users.

✉ Marcelo Machado Viana  
marcelo@gaiaresearch.com; marcelomachado@ufmg.br

<sup>1</sup> Department of Sanitary and Environmental Engineering, Federal University of Minas Gerais, P.O. Box 1294, Belo Horizonte, MG 30270-901, Brazil

<sup>2</sup> Department of Chemical Engineering, Pontifical Catholic University of Minas Gerais, P.O. Box 1686, Belo Horizonte, MG 30535-901, Brazil

<sup>3</sup> Department of Civil Engineering, Pontifical Catholic University of Minas Gerais, P.O. Box 1686, Belo Horizonte, MG 30535-901, Brazil

<sup>4</sup> Department of Physics and Chemistry, Pontifical Catholic University of Minas Gerais, P.O. Box 1686, Belo Horizonte, MG 30535-901, Brazil

<sup>5</sup> Department of Chemistry, Federal University of Minas Gerais, P.O. Box 1294, Belo Horizonte, MG 30270-901, Brazil

## Introduction

Pharmaceutical compounds are an important tool to recover and maintain human and animal health, being used for the most diverse purposes (Renita et al. 2017). They can be classified in several categories, for example: antiinflammatory, antipyretics, analgesics, antibiotics, antidepressants, chemotherapeutic agents, and contraceptives (Ikehata et al. 2006). Besides that, these compounds have been recognized as emerging pollutants due to their extensive use and long-term effects towards aquatic environment (Ashfaq et al. 2016; Pavithra et al. 2017). Furthermore, in aquatic environments they may have high persistence (Al-Gheethi et al. 2018), low biodegradability (Marcelino et al. 2016; Rana et al. 2017), and facile bioaccumulation (Ahmed and Hameed 2018). As a result, their occurrence in the environment became recurrent, in concentrations ranging from  $\text{ng L}^{-1}$  up to  $\mu\text{g L}^{-1}$ , as free compounds and/or as metabolites in many matrices worldwide, including drinking water supplies, wastewater effluents, soils, and sediments (Ebele et al. 2017; Senthil Kumar and Saravanan 2018; Reis et al. 2019; Prasannamedha

and Kumar 2020). Pharmaceutical compounds removal from aqueous media depends on the treatment employed in waste and drinking water treatment plants. A previous study (Reis et al. 2019) evaluated 28 pharmaceuticals in different drinking water treatment plants located in Brazil, one particular finding was that only part of the compounds considered were removed by conventional treatment (primary and secondary treatments).

Norfloxacin (NOR), an antibiotic from the fluoroquinolone's family, has extensive application in medical and veterinary practice (Van Doorslaer et al. 2014). Antibiotics are usually chemically stable compounds, which means that after administration to humans and animals, more than 90% of the drug can be excreted unchanged (Pouretedal and Sadegh 2014; Santos et al. 2015). Associated with this fact, the global pharmaceutical consumption in 2020 is expected to reach 4.5 trillion doses, representing a 24% increase over 2015 (Aitken 2015). This aggravates NOR presence in wastewaters originated from hospitals, households, and pharmaceutical industries, which is a major cause of the resistant bacteria emergence and acute and chronic toxicity (Prutthiwanasan et al. 2016). When assessing the presence of pharmaceutical and personal care products in water matrices of the Luomahu Lake (China), Zhang et al. (2017) reported NOR concentrations ranging from 256 to 707 ng L<sup>-1</sup>. In addition, the authors reported a moderate risk to aquatic ecosystem due to the pharmaceutical compound presence. Another research (Pereira et al. 2015) evaluated the occurrence of fluoroquinolones and tetracycline antibiotics in a Portuguese aquaculture system, reporting the NOR presence and a hazard quotient higher than one (meaning that adverse health effects are possible, but not certain). In this context, effective and efficient removal techniques are necessary. Among various methods currently proposed to remove pharmaceuticals from water matrices are ozonation (Gomes et al. 2017), intensified degradation (Nachiappan et al. 2018), membrane separation process (Foureaux et al. 2019), photocatalysis (El-Shafai et al. 2019; Prabavathi et al. 2019), electrocoagulation (Nariyan et al. 2017), biodegradation (Martins et al. 2018), and adsorption (Delgado et al. 2019).

Generally, in surface waters, biotic and abiotic mechanisms are responsible for this compound removal. Fluoroquinolones can be considered not biodegradable, given that 70% of NOR treated in conventional biological processes remained unchanged, although adsorbed to the sludge (Cardoza et al. 2005; Santos et al. 2015). Among the abiotic mechanisms are the adsorption process, indirect photodegradation, and hydrolysis (Babić et al. 2013). Regarding fluoroquinolones, photolysis and adsorption mechanisms predominate. These antibiotics exhibit different aromatic rings, heteroatoms, and other chromophore groups in their structure capable of absorbing solar irradiation, resulting in their photo-degradation and generating oxidant species like hydroxyl radicals and singlet

oxygen (Babić et al. 2013). Previous research (Santos et al. 2015) reported that NOR can be effectively degraded by Fenton, UV, and UV/H<sub>2</sub>O<sub>2</sub>, reaching removal efficiencies up to 100%. However, the authors reported that NOR mineralization resulted from these processes may lead to the recalcitrant compounds formation, whose toxic effects can have a greater impact on the environment than the original pharmaceutical (Santos et al. 2015).

Adsorption, on the other side, can be considered an economically, viable, and reliable alternative due to its simplicity in process design and reduced operation cost compared with other process (Zhang et al. 2017; Shen et al. 2019). Several adsorbents have been studied for pharmaceutical removal including microwave carbonized cellulose (Feng et al. 2018), activated carbon (Rostvall et al. 2018), biomass (Ahsan et al. 2018), and microalgae (Ali et al. 2018). Although there are many adsorbent materials, some of them exhibits low adsorption capacity or low efficiency (Madadrang et al. 2012). Therefore, in recent years, tremendous effort has been made to the search for new materials and techniques.

Recently, the advances in nanotechnology and engineering allowed the development of promising adsorbents for the removal of various contaminants such as heavy metals and organic molecules from water, including graphene and graphene oxide (GO) (Senthil Kumar and Saravanan 2019). Graphene is a two-dimensional material, with a hexagonal structure and sp<sup>2</sup> carbons, having high resistance and electrical transport, is highly promising with numerous applications, such as its use in molecular electronic devices, energy storage devices, desalination process, and many other applications. Graphene oxide (GO), on its turn, is an alternative material obtained after an oxidation and exfoliation process of expanded graphite which has excellent electrical and mechanical properties (Chowdhury and Balasubramanian 2014), high surface area (Cortés-Arriagada and Toro-Labbé 2016), good functionalizability, and dispersibility (Sheng et al. 2018). The use of GO as adsorbent has attract attention due to its structure which contains functional groups such as carboxylic acids and alcohols mainly located on the edges of GO, whereas hydroxyl and epoxide groups are located on its basal plane (Konicki et al. 2017; Sheng et al. 2018). All these functional groups can serve as pollutant binding sites, thus increasing the adsorption capacity. Moreover, due to GO structure and composition, hydroxyl radicals may also be formed under appropriate experimental conditions, which would contribute as simultaneous and complementary mechanisms for organic pollutants degradation.

Voylov et al. (2016) have shown a first example of controlled radical polymerization induced by free radicals generated during the GO reduction at 75 °C in aqueous media. The authors found an excellent polydispersity control, suggesting that using GO as a radical initiator is a new approach to radical polymerization and polymer composites preparation. The GO

reduction mechanism involving the oxygen removal has been proposed by Acik et al. (2011). In this chemical reaction, some hydroxyl radicals (OH•) and other free radicals could be produced considering the presence of trapped water between the nanosheets, decarboxylation reaction, and the continuous attack on hydroxyls as well as ring-opening of epoxides present in GO basal plane defects and sheet edges. The GO nanosheets reduction could occur even at room temperature and is more favorable with increasing temperature. A reduced graphene oxide/magnetite material was tested by Tang et al. (2013) for its applicability as adsorbent for antibiotics remediation. The results showed a strong process dependence on the medium pH reporting a maximum adsorption capacity of 22.22 mg g<sup>-1</sup> for norfloxacin. Peng et al. (2018) synthesized a reduced graphene oxide/Fe<sub>3</sub>O<sub>4</sub> nanocomposite for the simultaneous adsorption and degradation of norfloxacin. These authors found a maximum removal capacity of 158.1 mg g<sup>-1</sup>.

Although there are some studies reporting norfloxacin degradation and adsorption by carbonaceous materials such as reduced graphene oxide, to the best of our knowledge, there is not a detailed mechanistic and kinetic aspects of simultaneous NOR adsorption and degradation by GO. In this work, GO nanosheets was synthesized, and its ability to remove NOR through an intensified process involving adsorption-degradation by hydroxyl radicals was investigated.

## Materials and methods

### Chemicals and reagents

Expandable flake graphite (CAS 12777-87-6) was purchased from Asbury Graphite Mills, Inc. Phosphoric acid (H<sub>3</sub>PO<sub>4</sub>), sulfuric acid (H<sub>2</sub>SO<sub>4</sub>), potassium permanganate (KMnO<sub>4</sub>), hydrogen peroxide (H<sub>2</sub>O<sub>2</sub>), hydrochloric acid (HCl), and norfloxacin were purchased from Sigma-Aldrich (St. Louis, MO, USA). All reagents were analytical grade and used without further purification. Ultrapure water (0.057 μS cm<sup>-1</sup>) was used for solutions preparation. When necessary, the solutions pH was adjusted with hydrochloric acid (0.1 mol L<sup>-1</sup>) or sodium hydroxide (0.1 mol L<sup>-1</sup>).

### Graphene oxide preparation

After the thermal expansion of the expandable graphite at 800 °C for 30 min in a furnace, the expanded graphite (EG) obtained was employed to prepare the GO sample. The next steps of the experimental procedures were carried out according to modified Hummers method (Marcano et al. 2010). Firstly, 50 mg of expanded graphite powder was mixture to sulfuric acid and phosphoric acid solution, in the 9:1 volume ratio, respectively. The dispersion obtained was maintained under magnetic stirring at 100 °C for 2 h. Subsequently,

potassium permanganate was added to the mixture in the graphite: KMnO<sub>4</sub> mass ratio of 1:5. The system was again heated under stirring at 50 °C for 1 h. In the next step, 50 mL of distilled water was added, and the mixture was sonicated for 2 h. Then, 20 mL of hydrogen peroxide (30% v/v) was added to this dispersion. The dispersion was then centrifuged for 5 min at 3500 rpm, the supernatant was removed sequentially, and a volume of hydrochloric acid (HCl 10% v/v) equal to that of distilled water used in the last step was added. Finally, the dispersion was rinsed with distilled water until neutralization (pH ~ 6), and the brown powder obtained was dried by freeze drying.

### Graphene oxide characterization

X-ray diffraction (XRD) patterns collected at a scanning rate of 2° min<sup>-1</sup> were carried out on a Rigaku D/Max 2550 diffractometer equipped with a CuK<sub>α</sub> radiation source (λ = 1.5418 Å) set to 40 kV at 30 mA. The average number of graphene sheets was determined by using the Debye-Scherrer equation (Eq. 1) (Bera et al. 2018):

$$t = \frac{0.89 \lambda}{\beta_{002} \cos \theta_{002}} \quad (1)$$

$$n = \frac{t}{d_{002}} \quad (2)$$

where  $t$  is the thickness of layers,  $\beta$  is the full width at half maxima (FWHM),  $n$  (Eq. 2) is the number of layers,  $d$  is the interlayer spacing and  $\theta$  is the diffraction angle. SEM micrographs were taken on a Quanta 200 FEG-FEI microscope and TEM images were obtained in a FEI Tecnai G2–20 microscope with tungsten filament at 200 kV. The GO sample was deposited on 300 mesh copper grid Holey Carbon type. The chemical composition of graphite, GO and GO after adsorption was analyzed by X-ray photoelectron spectroscopy (XPS), using a K-Alpha X-ray photoelectron spectrometer (Thermo Fisher Scientific) equipped with hemispherical electron analyzer and monochromatic Al K<sub>α</sub> (1486.6 eV) radiation. The incident radiation diameter was maintained at 400 μm throughout the experiment. Survey scans were performed using a 200-eV pass energy, while carbon, oxygen, fluorine, and nitrogen high-resolution scans were obtained with 50 eV pass energy with resolutions of 1.0 and 0.1 eV, respectively. The data were analyzed and the peak deconvolution was performed using the Thermo Avantage Software. Chemical structure of GO, before and after adsorption experiment, was also analyzed using Fourier transformation infrared spectroscopy (FTIR).

Specific surface area was assessed by N<sub>2</sub> gas adsorption technique (QuantaChrome/NOVA 1200e), employing the BET methodology. FTIR spectra were obtained with a Thermo Scientific Nicolet 380 FT-IR using KBr pellets, under

ambient conditions. The spectra were obtained in the wave-number range from 4000 to 450  $\text{cm}^{-1}$ . Typically, 64 scans at a resolution of 4  $\text{cm}^{-1}$  were accumulated for each spectrum.

## Batch adsorption studies

### pH effect

The pH effect on the adsorption-degradation process was established according to the following conditions: initial NOR concentration = 30  $\text{mg L}^{-1}$ ; GO concentration = 200  $\text{mg L}^{-1}$ ; temperature = 303 K; 4 h of contact time and pH varying from 2 to 10. Further experiments were conducted under the most appropriate pH conditions. The point of zero charge (pHpzc) was determined as described elsewhere (Bian et al. 2015).

### Equilibrium isotherm

Equilibrium was investigated in 50-mL amber glass test tubes, where 10 mL of a solution containing 200  $\text{mg L}^{-1}$  GO, pH 7 and different NOR concentrations (10–90  $\text{mg L}^{-1}$ ) was placed under constant agitation (250 rpm) and temperature (303 K) in an orbital shaker (Marconi MA420) for 4 h. Afterwards, samples (5 mL) were taken and filtered through a 0.45  $\mu\text{m}$  PVDF syringe filter (CHROMAFIL® Xtra), and the NOR concentration was determined by a molecular absorption spectrometer (UV-Vis, Shimadzu UV 3600) and an external calibration curve (0.5–15  $\text{mg L}^{-1}$ ,  $R^2 > 0.99$ ). The adsorption capacity  $q_e$  ( $\text{mg g}^{-1}$ ) was calculated by Eq. S1 (supplementary material). To model the experimental equilibrium data, four isotherms models were fitted: Langmuir (Eq. S2), Freundlich (Eq. S4), Temkin (Eq. S5), and Sips models (Eq. S6). Control runs (same experimental condition, but without GO) were carried out to assess possible adsorption or degradation other than by GO. In these runs, no significant decrease in NOR concentration was observed.

The best fitted model was used to predict the  $q_e$  ( $\text{mg g}^{-1}$ ) given a specific equilibrium concentration in a single stage batch reactor as proposed in a previous study (Lebron et al. 2019). GO applicability for NOR remediation in an industrial scale was assessed after solving the material balance for this reactor, in which a scheme is given in supplementary Fig. S1. All equations involving the material balance for the scale up analysis is given in Eqs. S26–S27.

### Kinetics studies

The effect of contact time was investigated through kinetics parameters. In this case, the adsorption experiments were carried out in 125-mL Erlenmeyer flasks covered with tin foil under the following conditions: 200  $\text{mg L}^{-1}$  of GO, pH 7 and 30  $\text{mg L}^{-1}$  of NOR. The systems were kept under constant

agitation (250 rpm) and temperature (303 K). Aliquots (2 mL) were collected and filtered through a PVDF syringe filter at specific time intervals (0, 0.5, 1, 2, 5, 10, 15, 30, 60, 140, and 240 min). Then, the uptake capacity at respective time  $q_t$  ( $\text{mg g}^{-1}$ ) (Eq. S7) was estimated.

The pseudo first order model (PFO, Eq. S8), proposed by Lagergren, and the pseudo second order model (PSO, Eq. S9), proposed by Ho and McKay, were fitted to the kinetic experimental data. Furthermore, Weber and Morris (Eq. S11) and Boyd (Eq. S12–14) models were used to comprehend the adsorption mechanism in terms of intraparticle diffusion as a control stage. Complementing Weber and Morris and Boyd's model, Fick's law (Eq. S15) was employed to determine both film and intraparticle diffusion coefficient.

### Thermodynamics studies

The temperature effect on the adsorption process was investigated by conducting experiments at different temperatures (304, 314, 324, and 334 K) under the following conditions: 200  $\text{mg L}^{-1}$  of GO, pH 7, and 30  $\text{mg L}^{-1}$  of NOR. The system remained under constant agitation (250 rpm) for 240 min. Gibbs free energy change ( $\Delta G^\circ$ ), entropy change ( $\Delta S^\circ$ ), and enthalpy change ( $\Delta H^\circ$ ) were evaluated from Eq. S19 and Eq. S20.

### Norfloxacin intermediates identification

After adsorption tests, the intermediates products derived from the degradation process of the NOR were identified with a micrOTOF-QII mass spectrometer (Bruker) by direct infusion, adopting a dry gas flow rate of 7.0  $\text{L min}^{-1}$  and dry heater temperature of 180  $^\circ\text{C}$  for the electrospray ionization (ESI+). MS data were recorded in the full scan mode (from 50 to 2000  $m/z$ ), and nitrogen ( $\text{N}_2$ ) was used as nebulizer and collision gas. Instrument control, data acquisition, and subsequent analysis were conducted in Compass DataAnalysis version 4.2 software.

### Model fit statistics

The isotherm and kinetic parameters were estimated through Origin 2018 software (OriginLab, USA) minimizing the chi-square function. Five parameters were considered in order to assess the best experimental data fit. They are determination coefficient ( $R^2$ , Eq. S21) sum of error square (SSE, Eq. 22), composite fractional error function (CFEF, Eq. S23), chi-square statistic ( $\chi^2$ , Eq. S24), and average relative error (ARE, Eq. S25). Low values of SSE, CFEF,  $\chi^2$ , and ARE, in addition to  $R^2$  values close to unity, indicate a good experimental data fit to the proposed models.



## Results and discussion

### Graphene oxide characterization

Figure 1a shows the diffractograms for expanded graphite (EG) and graphene oxide (GO). The characteristic diffraction peak at  $2\theta = 26.4^\circ$  corresponds to an interlayer distance  $d_{002}$  of 0.33 nm assigned to the stacking of graphene sheets in graphite structure (Viana et al. 2015). After the acid and ultrasonic treatment, the  $26.4^\circ$  peak vanished and a peak at  $10.7^\circ$  (interplanar distance of 0.86 nm) is observed, evidencing the oxidation and exfoliation process associated to GO preparation. The average number of layers ( $n$ ) to EG and GO was estimated using the FWHM and the values found were 61 sheets and 8 sheets, respectively.

The chemical composition and the atomic percentage of the graphitic surfaces determined from XPS survey spectra are shown in Fig. 1b. The expanded graphite showed carbon

(C1s) and a small percentage of oxygen while greater quantities of oxygen element were observed in GO, confirming the graphitic structure oxidation. Besides of oxygen (O1s), photoemission peaks for fluorine (F1s), and nitrogen (N1s) from NOR molecule were observed for GO sample analyzed after the adsorption experiment.

Figure 1c, d also shows the SEM and TEM images for EG and GO samples. The interlayer expansion promoted at  $800^\circ\text{C}$  by intercalation compounds exists in graphite led to the formation of expanded graphite with an open and porous structure (Fig. 1c) and specific volume of  $150\text{ cc g}^{-1}$ . TEM image showed in Fig. 1d evidenced the presence of few GO sheets presents in a micrometric structure containing some folds. TEM result corroborates the number of sheets found by XRD technique.

The BET analysis demonstrated that the GO sample has an specific surface area (SSA) of  $67\text{ m}^2\text{ g}^{-1}$ , a value validated by the C constant of 38 ( $0.05 < P/P_0 < 0.3$ ) and the linear

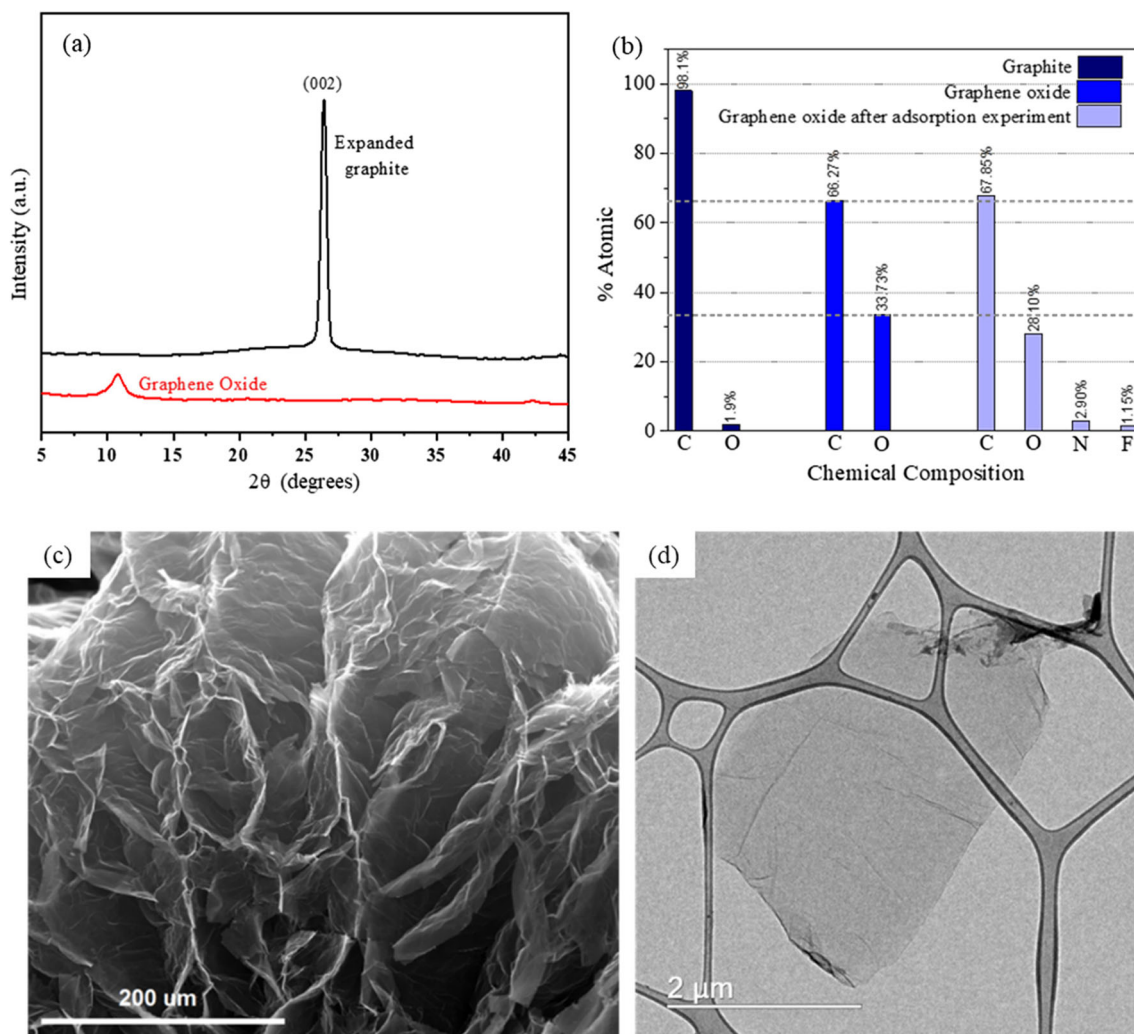


**Fig. 1** a XRD patterns of graphene oxide and expanded graphite, b X-ray photoelectron spectroscopy (XPS) results for expanded graphite, graphene oxide, and graphene oxide after adsorption studies in terms of

chemical composition, c SEM image for expanded graphite, and d TEM image of a GO sheet

coefficient correlation ( $r$ ) above 0.999 (Gregg et al. 1967; Thommes et al. 2015). The relatively low SSA, compared with activated charcoal, suggests that the GO nanosheets has a high degree of layer ordering maintaining low structural distortion due to  $sp^3$  carbon presence, and reveals the occurrence of a preferential oxidation process at the nanosheet edges (Gurzęda et al. 2017). The result of SSA was higher than other studies which demonstrates that the material synthesized has a great potential for adsorption process. For example, Bele et al. (2016) reported a GO with a specific surface area of  $20.93 \text{ m}^2 \text{ g}^{-1}$ .

The XPS analysis was carried out to evaluate the chemical bonds present in the graphite (Supplementary Fig. S2), in the GO and, therefore, confirm if the chemical modifications occurred in GO after adsorption experiment. Fig. 2a, b shows XPS core-level spectra of (a) C1s and (b) O1s for GO. The C1s of GO consists of five different chemically shifted components and can be deconvoluted into C=C, C–C, C–O, C=O and –COOH. For O1s of GO, the presence of oxygenated functions is observed as C=O, C=O, O–H, C–O–C, and C–O groups and H<sub>2</sub>O. These assignments agree with previous work (Ganguly et al. 2011; Viana et al. 2015; Yu et al. 2016) and are presented by Table 1.

Chemical modifications occurred in GO after adsorption experiment as shown in XPS core-level spectra of C1s (Fig. 3a) and N1s (Fig. 3c). The presence of the C–F and C–N in C1s spectrum confirms the adsorption of NOR onto the GO surface. After the adsorption experiment, nitrogenous functions appear which are identified in the spectrum of N1s. The presence of –NH, N= is attributed to NOR, and these assignments agree with previous work (Pang et al. 2010). However, peaks attributed to N–C=O, N+ and nitrogen oxides were also observed. Fig. 3b shows O1s of graphene oxide. The presence of oxygenated functions is observed as C=O, C=O, O–H, C–O–C, C–O groups, and H<sub>2</sub>O. Amide and nitrogen oxide groups also were observed for graphene oxide

**Table 1** Binding energy and percentage of compounds from C1s and O1s XPS spectra for graphene oxide (Ganguly et al. 2011; Viana et al. 2015; Yu et al. 2016)

	Assignment	Binding Energy (eV)	Atomic %
C1s	C=C	284.4	10.39
	C–C	285.5	25.60
	C–O	286.5	9.74
	C=O	287.5	49.46
	–COOH	289.3	4.81
O1s	C=O	530.5	3.24
	C=O, O–H, C–O–C	532.0	14.98
	C–O	533.3	75.19
	H <sub>2</sub> O	534.7	6.60

after adsorption experiment. Assignment, binding energy, and atomic% from O1s XPS spectra are presented by Table 2.

The FTIR spectra and the characteristic bands of norfloxacin, graphene oxide, and graphene oxide after adsorption experiments are shown in Fig. 4. The assignments presented for graphene oxide (Fig. 4a) and norfloxacin (Fig. 4c) agree with previous work (Sahoo et al. 2012; Yu et al. 2016). The bands at  $2506\text{--}3049 \text{ cm}^{-1}$  (region I) in the curve of norfloxacin are attributed to the  $\text{--}^+\text{NH}_2$  vibration (Shi et al. 2016). These bands vanished after the adsorption experiments as can be observed in the Fig. 4b. The intensification/appearance of some vibration bands in region II and region III corroborated the XPS results confirming the degradation of norfloxacin (Table 3).

The XPS results and FTIR spectra for GO-NOR sample have evidenced the appearance of spectroscopy signals related to NO<sub>x</sub> compounds and the N–C=O amide groups associated to byproducts and the vanishing of some signals related to the piperazinyl moiety presence suggesting that the NOR molecule was degrading during the experiments of adsorption. The

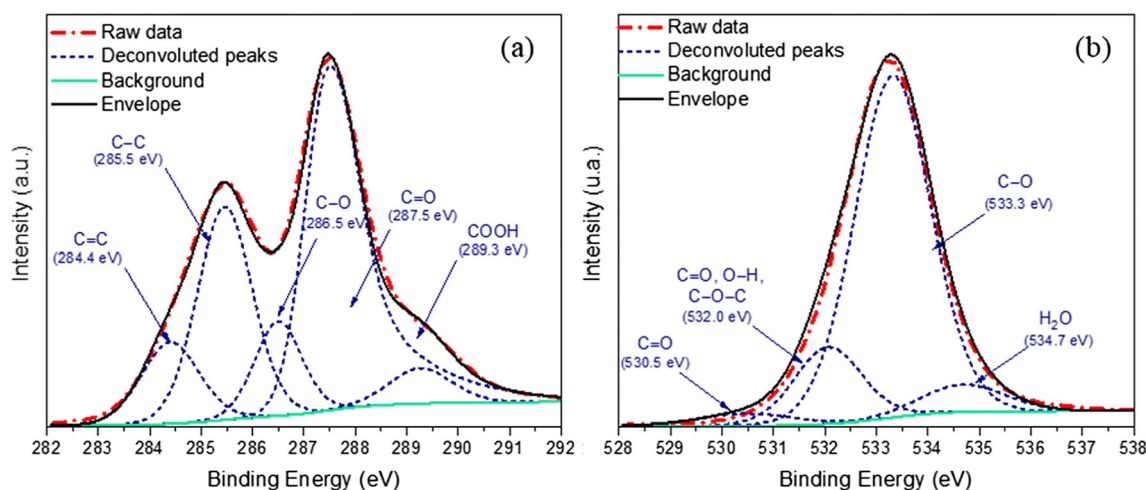


**Fig. 2** XPS core-level spectra of **a** C1s and **b** O1s for graphene oxide as prepared

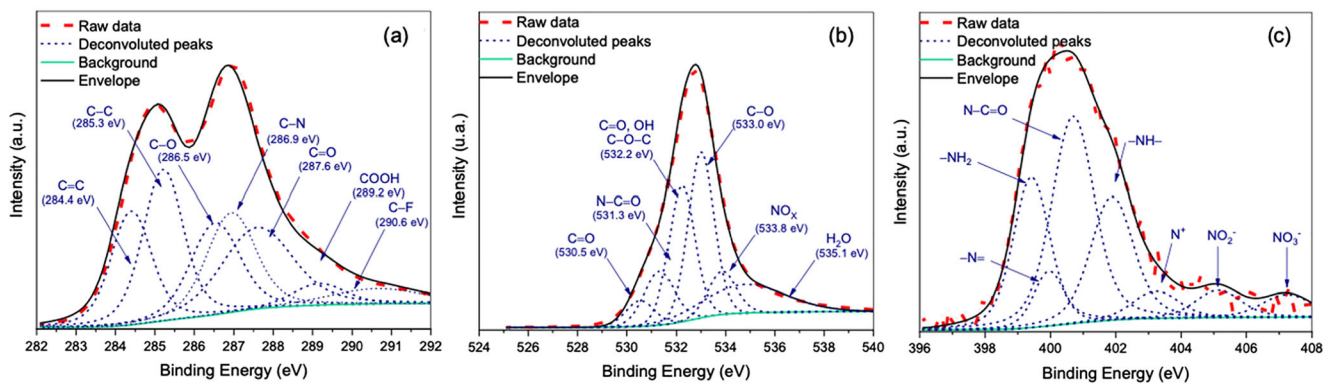


**Fig. 3** XPS core-level spectra of **a** C1s, **b** O1s and **c** N1s for graphene oxide after adsorption experiment

amide and nitrogen oxide groups also were observed on O1s XPS spectra for GO after adsorption experiment (Fig. 3) and reinforce this proposal. The temperature of the sonication bath used to disperse GO nanosheets, which in our method could reach up to 60 °C, combined to cavitation process promoted the free radical’s formation from GO structure. It is important to note that in control runs, where the system was put under the same operational conditions but without the GO presence, no significant decrease in NOR concentration was observed. Furthermore, Ola and Erland (2015) assessed the thermal stability of different antibiotics in aqueous solutions for

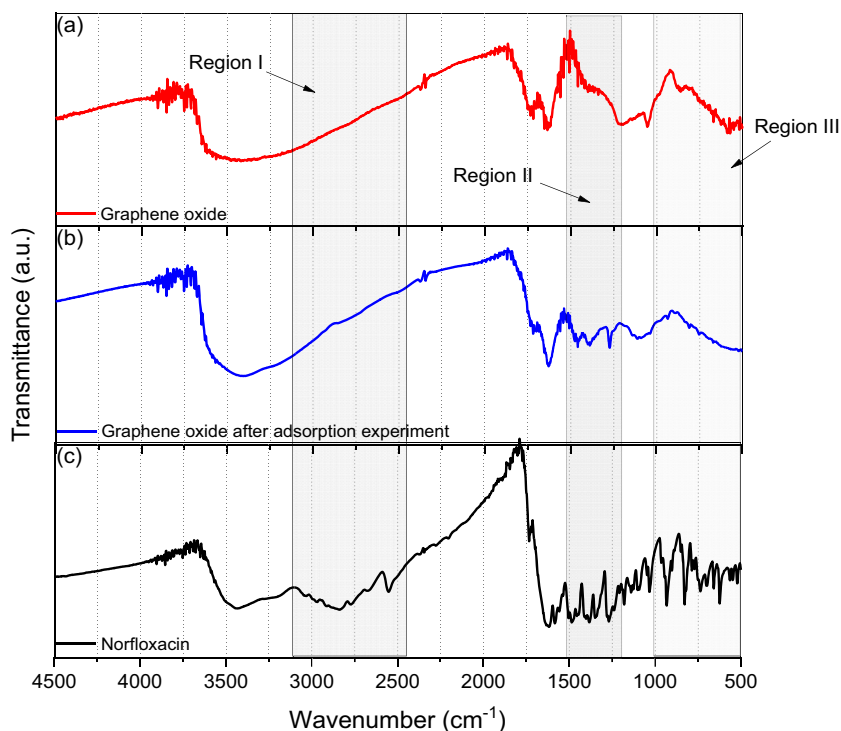
moderated temperature, including norfloxacin, which showed a remarkably high thermal stability for temperatures up to 200 °C. Moreover, NOR stability to ultrasonication was previously reported (Ma et al. 2018). In this study, a low degradation kinetic constant ( $k = 0.00019 \text{ min}^{-1}$ ) was reported, and after 30 min of ultrasonication, approximately 99% of NOR was still stable. Therefore, most degradation and removal of NOR observed throughout our study were related to its degradation by hydroxyl radicals or GO sequestration.

**Table 2** Binding energy and percentage of compounds from C1s, O1s, and N1s XPS spectra for graphene oxide after adsorption studies (Polishchuk et al. 2009; Pang et al. 2010; Ganguly et al. 2011; Viana et al. 2015; Yu et al. 2016)

	Assignment	Binding energy (eV)	Atomic %
C1s	C=C	284.4	16.22
	C–C	285.3	21.51
	C–O	286.5	15.84
	C–N	286.9	17.17
	C=O	287.6	20.33
	–COOH	289.2	3.94
	C–F	290.6	5.00
O1s	C=O	530.5	5.73
	N–C=O	531.3	12.54
	C=O, O–H, C–O–C	532.2	24.99
	C–O	533.0	38.53
	NO <sub>x</sub>	533.8	9.38
	H <sub>2</sub> O	535.1	8.84
N1s	NH <sub>2</sub>	399.42	22.11
	N =	399.95	6.68
	N C = O	400.69	35.47
	N H	401.88	21.24
	N <sup>+</sup>	403.22	5.06
	NO <sub>2</sub> <sup>–</sup>	405.13	5.03
	NO <sub>3</sub> <sup>–</sup>	407.24	4.41

In our study, the radical formation hypothesis due to the conditions previously mentioned was supported by XPS analysis. Complementarily, NOR molecules degradation was confirmed by different intermediates (Table 4), identified by their respective molecular and mass fragment ions obtained by mass spectrum (Supplementary Fig. S3) and compared with different studies available in the literature. In general, processes involving organic contaminants degradation via OH• radicals are highly active and non-selective, which results in several intermediates (Gou et al. 2017). Chen and Chu (2016) divided the degradation mechanism into two different stages, starting with the attack of hydroxyl radicals on the benzene and piperazine rings, leading to formation of the intermediates I<sub>1</sub> and I<sub>2</sub>, also identified in this study. The presence of OH• radicals and their reaction with the intermediates I<sub>1</sub> and I<sub>2</sub> would justify the observation of I<sub>3</sub>, I<sub>4</sub>, I<sub>5</sub>, and I<sub>6</sub>, derived from carbon-centered radicals formed when an OH• radical gets an electron via bond cleavage or H abstraction (Kleiser and Frimmel 2000; Chen and Chu 2016). This in turn possesses the ability to rapidly react with oxygen promoting the organic peroxy radical’s formation, which in turn undergo self-reaction and generate aldehydes, ketones, and/or carbon dioxide. Other byproducts were also identified, corresponding to intermediates I<sub>7</sub> and I<sub>8</sub>, which possible degradation mechanism was explored by Sayed et al. (2016). Intermediate I<sub>9</sub> was also identified by Ding et al. (2017). According to the authors, NOR molecule degradation would occur mainly by the attack of radicals on piperazinyl and quinolone moieties, and the formation of the intermediate would be associated with a route involving a defluorination reaction. Similarly,

**Fig. 4** FTIR spectra of **a** norfloxacin; **b** graphene oxide; and **c** graphene oxide after adsorption experiment



intermediate  $I_{10}$  was also identified by Gou et al. (2017) deriving from a defluorination reaction. Additionally, the molecular ion  $m/z$  362.4 was also recurrent in the mass spectra presented by Zhang et al. (2018) after norfloxacin degradation by graphene oxide-supported cobalt phthalocyanine, however, not composing the degradation mechanism proposed by the authors. Lastly, none of the ions were found in the NOR spectrum before degradation-adsorption process (Supplementary Fig. S4).

## Batch adsorption studies

### pH effect

Depending on the solution pH, NOR can exist in different microspecies cationic ( $\text{NOR}^+$ , microspecies#1), zwitterionic ( $\text{NOR}^\pm$ , microspecies#3), and anionic form ( $\text{NOR}^-$ , Microspecies#2), all of which represented in Fig. 5. In general, pH effects on adsorption capacity correlated well with the NOR speciation diagram, where the highest adsorption

capacity was obtained was around pH 7 ( $150.38 \text{ mg g}^{-1}$ ). Using Eq. 3, it is possible to identify the different species contribution to the overall NOR adsorption.

$$q_e = q^+ \gamma^+ + q^- \gamma^- + q^\pm \gamma^\pm \quad (3)$$

where  $q^+$ ,  $q^-$ , and  $q^\pm$  are the adsorption amounts for cationic, anionic, and zwitterionic NOR. The  $\gamma^+$ ,  $\gamma^-$ , and  $\gamma^\pm$  are the fraction of cationic, anionic, and zwitterionic NOR at certain pH, respectively. Supplementary Table S2 shows the greater zwitterionic form contribution to the total adsorption capacity, which can also be perceived by Fig. 5, since increasing the  $\text{NOR}^\pm$  fraction the adsorption capacity increased.

Adsorption process involving carbon nanomaterials as adsorbent is directly related to the charge density presented by the adsorbate associated to the formation of hydrogen-bond donor and acceptor and  $\pi$ - $\pi$  interactions between adsorbate-adsorbent. In our study, the  $\text{NOR}^\pm$  fraction adsorbed is considerably higher than other species since this structure have the higher charge density, favoring the adsorption process. Furthermore, this result is in accordance with the material pH<sub>pzc</sub> (pH<sub>pzc</sub> = 3.9, Supplementary Fig. S5). It is important to note that in pH > pH<sub>pzc</sub> the GO surface would be mostly negatively charged, in which the uptake of microspecies #1– $\text{NOR}^\pm$  (predominant under that pH condition) would be favored. Similar results were found by Yang et al. (2012) which evaluated the NOR adsorption onto porous resins and carbon nanotube. These and other authors also found a higher NOR adsorption capacity at pH around 7 (Samiee et al. 2019).

**Table 3** Vibrational spectrum of nitrogen oxide species. (Brooker and Irish 1968)

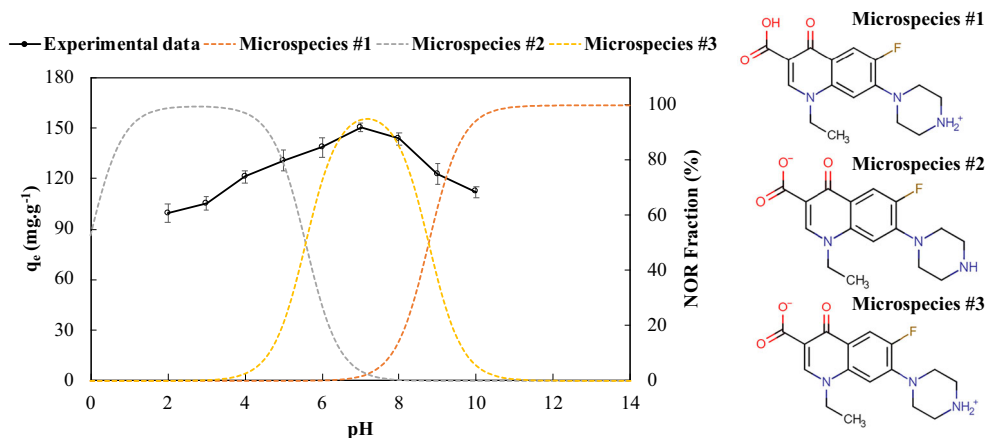
	Assignment	Wavenumber ( $\text{cm}^{-1}$ )
Observed frequencies	$\nu_3 \text{NO}_2^-$	1240
	$\nu_1 \text{NO}_3^-$	1330
	$\nu_3 \text{NO}_3^-$	1387



**Table 4** Intermediates identified after norfloxacin molecule degradation. ( $n = 3$ ;  $C_0 = 30 \text{ mg L}^{-1}$ ;  $GO = 200 \text{ mg L}^{-1}$ ; temperature = 303 K; contact time = 4 h)

Intermediates	Molecular ion $[M+H]^+$	Calculated (m/z) $[M+H]^+$	Chemical Structure	Proposed Formula
Norfloxacin	320.1432	320.1404		$C_{16}H_{19}FN_3O_3$
I <sub>1</sub>	314.1460	318.1448		$C_{16}H_{20}N_3O_4$
I <sub>2</sub>	334.1653	334.1397		$C_{16}H_{20}N_3O_5$
I <sub>3</sub>	324.1905	324.1190		$C_{14}H_{18}N_3O_6$
I <sub>4</sub>	294.1577	294.1248		$C_{14}H_{17}FN_3O_3$
I <sub>5</sub>	261.1110	261.2172		$C_{13}H_{29}N_2O_3$
I <sub>6</sub>	233.0953	233.0920		$C_{12}H_{13}N_2O_3$
I <sub>7</sub>	251.1156	251.0826		$C_{12}H_{12}FN_2O_3$
I <sub>8</sub>	252.1354	252.0666		$C_{12}H_{11}FNO_4$
I <sub>9</sub>	274.4059	274.1550		$C_{15}H_{20}N_3O_2$
I <sub>10</sub>	301.1194	301.0481		$C_{17}H_7N_3O_3$

**Fig. 5** Speciation diagram and pH effect on norfloxacin adsorption. ( $n = 3$ ;  $C_0 = 30 \text{ mg L}^{-1}$ ;  $GO = 200 \text{ mg L}^{-1}$ ; temperature = 303 K; contact time = 4 h)



Adsorption mechanism of NOR onto GO was mainly dominated by Van der Waals force and  $\pi$ - $\pi$  interaction. The interaction of hydrogen bond donor and acceptor (HDA) also contributed the adsorption since GO had oxygen carrying functional groups.

### Equilibrium isotherm

The equilibrium involving the process was assessed by four different models. Among them, Sips was selected for the process description based on the higher determination coefficient and lower error function values as reported in Table 5. Sips model assumes the monolayer formation onto the adsorbent surface; moreover, this model can be considered as a

combination of Langmuir and Freundlich isotherm (Inglezakis et al. 2018). The adsorbent had theoretical maximum adsorption capacity  $q_{mS} = 374.981 \pm 29.888 \text{ (mg g}^{-1}\text{)}$ , and its constant  $m_T$  ( $0.882 \pm 0.084$ ) was close to unity, which suggests an approximation of the model to the Langmuir isotherm. The latter assumes a finite number of energetically equivalent sites as well a homogeneous adsorbent surface, where the adsorption process occurs with the formation of a monolayer. Langmuir isotherm also adjusted satisfactorily to the observed data ( $R^2 = 0.993$ ) presenting an agreement between the parameters  $q_{mS}$  and  $q_m$ , which differed by only 10.6%. The suitability to Langmuir model is in accordance with the structure presented by GO, which is distributed in the form of overlapping layers. This would limit the multiple

**Table 5** Isotherm parameters obtained by nonlinear estimation for norfloxacin adsorption onto graphene oxide. Mean  $\pm$  standard error. ( $n = 3$ ;  $C_0 = 10\text{--}90 \text{ mg L}^{-1}$ ;  $GO = 200 \text{ mg L}^{-1}$ ; temperature = 303 K; contact time = 4 h)

Isotherm model	Parameter value	Isotherm model	Parameter value
Langmuir		Sips	
$q_m \text{ (mg}\cdot\text{g}^{-1}\text{)}$	$334.610 \pm 11.630$	$q_{mS} \text{ (mg}\cdot\text{g}^{-1}\text{)}$	$374.981 \pm 29.888$
$K_L \text{ (L}\cdot\text{mg}^{-1}\text{)}$	$0.238 \pm 0.027$	$K_S \text{ (L}\cdot\text{mg}^{-1}\text{)}$	$0.174 \pm 0.042$
$R_{L, \text{min}}\text{--}R_{L, \text{max}}$	$0.044\text{--}0.296$	$m_T$	$0.822 \pm 0.084$
$R^2$	0.993	$R^2$	0.997
SSE (%)	2.512	SSE (%)	2.077
CFEF	4.308	CFEF	0.977
$\chi^2$	5.075	$\chi^2$	0.953
ARE (%)	7.220	ARE (%)	3.169
Freundlich		Temkin	
$K_F \text{ (mg}^{1-1/n}\cdot\text{L}^{1/n}\cdot\text{g}^{-1}\text{)}$	$89.007 \pm 11.522$	$b \text{ (J mol}^{-1}\text{)}$	$38.995 \pm 2.253$
$n$	$2.703 \pm 0.338$	$A_T \text{ (L}\cdot\text{g}^{-1}\text{)}$	$3.372 \pm 0.601$
$R^2$	0.962	$R^2$	0.987
SSE (%)	3.950	SSE (%)	2.988
CFEF	16.393	CFEF	6.244
$\chi^2$	13.309	$\chi^2$	6.897
ARE (%)	13.433	ARE (%)	8.596
$q_{e, \text{exp}} \text{ (mg}\cdot\text{g}^{-1}\text{)}$	$296.771 \pm 6.479$		

layer formation process as described by Freundlich, therefore, restricting the formation of monolayers.

From the Langmuir fit is possible to suggest the process viability when the separation coefficient ( $R_L$ ) was taken into consideration ( $0 < R_L < 1$ ). The same can be said for parameter  $n$  obtained for the Freundlich model (constrained in the range of 0–10) meaning that small amounts of GO are capable to adsorb large NOR amounts. Freundlich model, in contrast with Langmuir, assumes a heterogeneous adsorbent surface, heterogeneity in the energy of the adsorption sites and a multilayer formation along the adsorption process (Bonilla-Petriciolet et al. 2017; Lebron et al. 2018; Moreira et al. 2019; Delgado et al. 2019). The models fit to the experimental data can also be observed in Fig. 6a, where smaller deviations between the curve and the experimental data were observed for the Sips and Langmuir models. A directly proportional relationship between the adsorption capacity and initial NOR concentration was observed, followed by a slightly decrease in its slope. However, it did not reach a constant value indicating that the active sites were not yet saturated.

**Kinetic studies**

The adsorption process was best described by the PSO model (Table S3), in which the equilibrium was achieved passed 30 min (Fig. 6b) after the process started, presenting an initial adsorption rate of  $4346.393 \pm 490.864$  ( $\text{mg g}^{-1} \text{min}^{-1}$ ). In several published papers, where the PSO presented a better fit to the experimental data, the authors directly associate that the adsorption process may occur due to chemisorption (Chen et al. 2008; Doyurum and Akyil 2011). Compared with the PFO model, it presented a higher determination coefficient and lower values for the error functions  $SSE$ ,  $CFEF$ ,  $\chi^2$ , and  $ARE$ . In addition to that, the value corresponding to the adsorption capacity calculated by the model was closer to the observed experimental value. The difference observed between the calculated and experimental adsorption capacity for the PFO model can be justified by its inability to describe the initial adsorption stages, where a time lag in the adsorbate uptake results from the boundary layer and external resistance.

When the adsorption mechanism was investigated, it was possible to observe the presence of more than one controlling stage in the NOR adsorption process by GO. From the fitted Weber and Morris model (Fig. 6c), it is possible to observe three linear sections, indicating the additional contribution of the mass diffusion in the boundary layer and confirmed by the non-zero constant  $c_0$  ( $95.728 \text{ mg g}^{-1}$ ). Furthermore, it is observed that  $K_{2,1 \text{ W\&M}} > K_{2,2 \text{ W\&M}} > K_{2,3 \text{ W\&M}}$ , explained by the initial active sites abundance, which became gradually occupied throughout the adsorption process and therefore reduced the adsorption rate. In addition to that, the higher NOR concentration in initial stages imposes an important driving force to overcome the mass transfer resistances between the

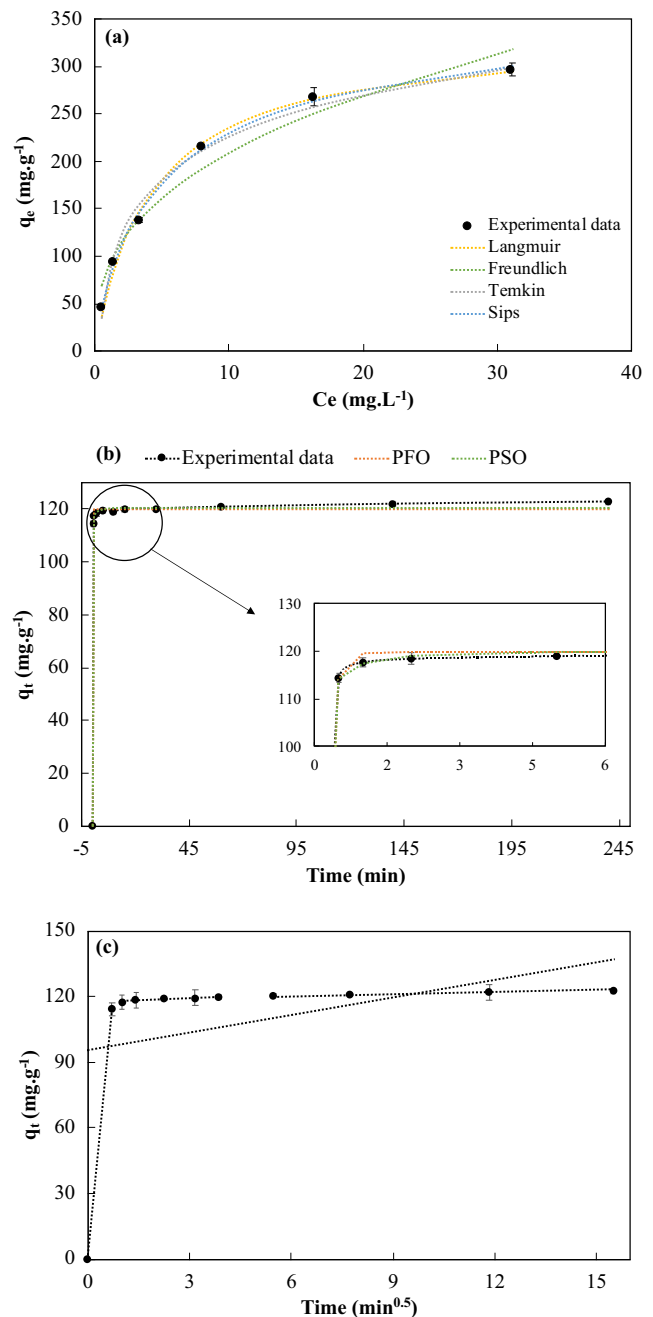


**Fig. 6** a Norfloxacin adsorption isotherm, experimental data, and fitted models, b pseudo-first order (PFO), pseudo-second order (PSO), and c Weber and Morris fit to the experimental data obtained

aqueous and solid phases, favoring the initial stages adsorption rate. The results obtained from the Weber and Morris model were confirmed by Boyd’s model fit which, even presenting a linear relation between  $B_t$  and  $t$  ( $R^2 = 0.991$ ), the plot did not intercept the origin.

The resistance to mass transfer through the boundary layer will depend on the system hydrodynamic conditions, directly affecting the boundary layer thickness surrounding the adsorbent particle. However, in practice and in the majority of real

**Table 6** Thermodynamic parameters values (mean  $\pm$  standard error,  $n = 3$ ) for norfloxacin adsorption onto graphene oxide. ( $n = 3$ ;  $C_0 = 30 \text{ mg L}^{-1}$ ;  $GO = 200 \text{ mg L}^{-1}$ ; temperature = 304–334 K; contact time = 4 h)

Adsorbate	T (K)	$\Delta G$ (kJ mol $^{-1}$ )	$\Delta H$ (kJ mol $^{-1}$ )	$\Delta S$ (kJ mol $^{-1}$ K $^{-1}$ )
Norfloxacin	304.15	$-7.784 \pm 0.036$	$-13.141 \pm 0.814$	$-0.018 \pm 0.003$
	314.15	$-7.608 \pm 0.011$		
	324.15	$-7.432 \pm 0.015$		
	334.15	$-7.256 \pm 0.041$		
<b>Model fit statistics</b>				
	$R^2$	0.992	$\chi^2$	0.001
	$SSE$ (%)	0.113	$ARE$ (%)	0.434

systems, mass transfer resistance in the pores is more significant than the resistance outside the particle (Nascimento et al. 2014). Considering the film ( $D_1$ ) and intraparticle ( $D_2$ ) diffusion coefficients obtained from Fick's law, it is observed that the latter is smaller which suggests that the intraparticle diffusion presents greater contribution as controlling stage of the adsorption process.

### Thermodynamic studies

As temperature changes, variations are expected in the adsorption rate, molecular interactions, and the solubility of the pharmaceutical compound. The NOR adsorption onto GO presented an exothermic character (Table 6), in which the adsorption capacity showed an inversely proportional behavior to the temperature (Supplementary Fig. S6). The enthalpy change value was lower than  $40 \text{ kJ mol}^{-1}$ , which suggests the existence of physical interactions. Furthermore, the process was spontaneous for the temperature range considered, with a reduction in the entropy during the adsorption process explained by a reduction in randomness between the solid-liquid interface of the system. The entropy results could be justified by the GO affinity for the NOR, which resulted in lower NOR

concentration in the liquid phase and as a consequence, a reduction in randomness between the solid-liquid interface.

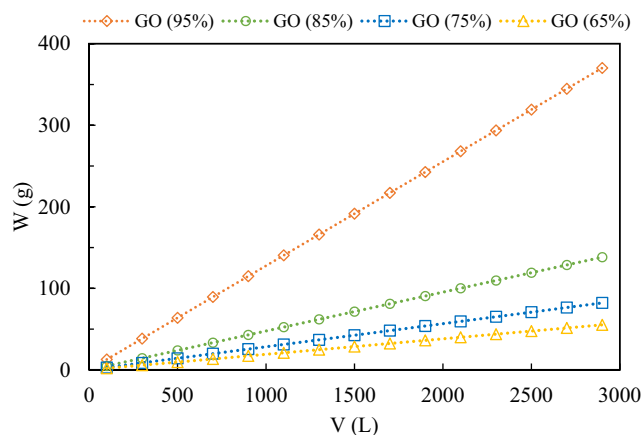
### Single stage batch design

Preliminary designs permit to extrapolate lab-bench-scale findings to a large scale, which could be further used in industrial wastewater treatment system designing. As discussed in the "Equilibrium isotherm" section, Sips was chosen as the most appropriate equilibrium model after fitted to the experimental data. Hence, this model was used to solve the material balance for a single stage batch design. A contaminated water containing  $1 \text{ mg L}^{-1}$  of NOR and removal efficiencies ranging from 65 to 95% was considered for the simulation, which results are shown in Fig. 7. For removal efficiencies up to 85%, there is a similar behavior for the increase in treated water volume to mass required, with an average increase of 15.85 g of GO for each 500 L of contaminated water. In the other side, considering the 95% removal efficiency, this GO mass requirement increases up to 75% (63.85 g of GO for each 500 L of contaminated water). This evidence shows the importance of taking into consideration scale up conditions while deciding for a suitable system, rather than isolated parameters. It is worth mentioning that the advances in large scale GO production (Stafford et al. 2018; Dong et al. 2018) allow the use of greater amounts of this material in benefit of water treatment.

### Recent advancements in GO as an adsorbent

Different studies involving GO as adsorbent for organic compounds' remediation are presented in Table 7. In addition to these, GO has already proven its efficiency for other pollutants treatment such as heavy metals (Samiee et al. 2019) and dyes (Kim et al. 2015). In most cases, the adsorption process was conducted in a synthetic aqueous medium in a batch mode configuration.

The present study presented substantial advancements regarding the NOR adsorption process, demonstrating the high

**Fig. 7** Single-stage batch design results: GO dosage ( $W$ ) vs volume of contaminated water ( $L$ )



**Table 7** Comparative studies involving adsorption of different organic compounds onto graphene oxide. All studies were carried out with synthetic aqueous solution and in batch mode operation. *n.r.*: not reported

Adsorbent	Adsorbate	Isotherm	Maximum adsorption capacity	pH	Temperature (K)	Kinetic	Thermodynamic nature of the process	Ref.
Graphene oxide	Norfloxacin	Sips	374.9 mg g <sup>-1</sup>	7.00	304	PSO	Exothermic: physisorption	This study
Graphene oxide nanosheets	17 β-estradiol	Langmuir	149.4 mg g <sup>-1</sup>	7.00	298	PSO	Exothermic: physisorption	(Jiang et al. 2016)
Graphene oxide	Naphthalene	Freundlich	21.4 mg g <sup>-1</sup>	5.00	298	n.r.	n.r.	(Wang and Chen 2015)
Graphene oxide	1-Naphthol	Langmuir	57.7 mg g <sup>-1</sup>	5.00	298	n.r.	n.r.	(Wang and Chen 2015)
Graphene oxide	Tetracycline	Langmuir	313.4 mg g <sup>-1</sup>	3.60	298	PSO	n.r.	(Gao et al. 2012)
Graphene oxide	Oxytetracycline	Langmuir	212.3 mg g <sup>-1</sup>	3.60	298	n.r.	n.r.	(Gao et al. 2012)
Graphene oxide	Doxycycline	Langmuir	398.4 mg g <sup>-1</sup>	3.60	298	n.r.	n.r.	(Gao et al. 2012)
Graphene oxide nanosheet	Sulfamethoxazole	Koble–Corrigan	127.0 mg g <sup>-1</sup>	7.00	298	PSO	Exothermic: chemisorption	(Rostamian and Behnejad 2016)

GO affinity for the NOR. The maximum adsorption capacity obtained was higher than that reported in available literature, although a different type of organic pollutant was considered among the studies. In most cases, the adsorption process is best represented by the Langmuir model as in the present study in which both Langmuir and Sips models were chosen to describe the process. Kinetic and thermodynamic parameters are commonly considered in different adsorption and also biosorption (Lebron et al. 2018; Moreira et al. 2019) process; however, it is forgotten in most of the studies dealing with pharmaceutical compounds. From these parameters, it is possible to understand the process viability, equilibrium time, and spontaneity. For the studies in which they were evaluated, a better adjustment was observed for the PSO model, in addition to an exothermic nature. Thus, an increase in the medium temperature would disadvantage the adsorption process, reducing its efficiency. Recycling and regeneration are still challenging in graphene oxide usage in water treatment processes. Zhang et al. (2014) proposed different solvents for bisphenol A desorption from reduced graphene oxide combined with magnetic nanoparticles. In this reference, desorption efficiency varied from approximately 40 to 98%, when cyclohexane and methanol was used, respectively, reporting an effective reusability until the fifth cycle.

## Conclusions

In the present research, GO was used as an adsorbent and simultaneously as a radical initiator for the norfloxacin antibiotic adsorption/degradation in water. Combined the results from XRD, XPS, FTIR, UV-Vis, SEM, and TEM, the superior

removal performance of GO can be attributed to norfloxacin degradation promoted by hydroxyl radicals formed in water. Adsorption process was best described by Sips and Langmuir isotherm, suggesting a single layer formation over an adsorbent homogeneous surface. The highest adsorption capacity was observed at pH 7, with a greater contribution of the norfloxacin zwitterionic species. Pseudo-second order model better fitted the process, presupposing chemical interactions throughout the adsorption process, achieving its equilibration after 30 min. The adsorption process was exothermic and spontaneous, indicating that the adsorption is more favorable at ambient temperature. Moreover, it can be concluded that the use of GO for removing emergent contaminants may be better exploited since there are an enormous potential of its application in the intensification of environmental remediation processes.

**Acknowledgments** The authors acknowledge UFMG - Microscopy Center for the microscopy images and Nanotechnology Laboratory (LNNano) by XPS measurements (Proposals XPS-24609 and XPS-24668).

**Funding information** The authors would like to thank the Fapemig, CNPq, and Capes (Finance code 001) Brazilian agencies for the financial support received.

## References

- Acik M, Lee G, Mattevi C, Pirkle A, Wallace RM, Chhowalla M, Cho K, Chabal Y (2011) The role of oxygen during thermal reduction of graphene oxide studied by infrared absorption spectroscopy. *J Phys Chem C* 115:19761–19781. <https://doi.org/10.1021/jp2052618>

- Ahmed MJ, Hameed BH (2018) Removal of emerging pharmaceutical contaminants by adsorption in a fixed-bed column: a review. *Ecotoxicol Environ Saf* 149:257–266. <https://doi.org/10.1016/j.ecoenv.2017.12.012>
- Ahsan MA, Jabbari V, Islam MT, Kim H, Hernandez-Viezas JA, Lin Y, Díaz-Moreno CA, Lopez J, Gardea-Torresdey J, Noveron JC (2018) Green synthesis of a highly efficient biosorbent for organic, pharmaceutical, and heavy metal pollutants removal: engineering surface chemistry of polymeric biomass of spent coffee waste. *J Water Process Eng* 25:309–319. <https://doi.org/10.1016/j.jwpe.2018.08.005>
- Aitken M (2015) The global use of medicines: outlook through 2020. Parsippany, NJ
- Al-Gheethi A, Noman E, Mohamed R et al (2018) Removal of pharmaceutically active compounds from contaminated water and wastewater using biochar as low-cost adsorbents, an overview. In: *Handbook of environmental materials management*. Springer International Publishing, Cham, pp 1–9
- Ali MEM, Abd El-Aty AM, Badawy MI, Ali RK (2018) Removal of pharmaceutical pollutants from synthetic wastewater using chemically modified biomass of green alga *Scenedesmus obliquus*. *Ecotoxicol Environ Saf* 151:144–152. <https://doi.org/10.1016/j.ecoenv.2018.01.012>
- Ashfaq M, Khan KN, Rasool S, Mustafa G, Saif-Ur-Rehman M, Nazar MF, Sun Q, Yu CP (2016) Occurrence and ecological risk assessment of fluoroquinolone antibiotics in hospital waste of Lahore, Pakistan. *Environ Toxicol Pharmacol* 42:16–22. <https://doi.org/10.1016/j.etap.2015.12.015>
- Babić S, Periša M, Škorić I (2013) Photolytic degradation of norfloxacin, enrofloxacin and ciprofloxacin in various aqueous media. *Chemosphere* 91:1635–1642. <https://doi.org/10.1016/j.chemosphere.2012.12.072>
- Bele S, Samanidou V, Deliyanni E (2016) Effect of the reduction degree of graphene oxide on the adsorption of Bisphenol a. *Chem Eng Res Des* 109:573–585. <https://doi.org/10.1016/j.cherd.2016.03.002>
- Bera M, Chandravati GP, Maji PK (2018) Facile one-pot synthesis of graphene oxide by sonication assisted mechanochemical approach and its surface chemistry. *J Nanosci Nanotechnol* 18:902–912. <https://doi.org/10.1166/jnn.2018.14306>
- Bian Y, Bian Z-Y, Zhang J-X, Ding AZ, Liu SL, Wang H (2015) Effect of the oxygen-containing functional group of graphene oxide on the aqueous cadmium ions removal. *Appl Surf Sci* 329:269–275. <https://doi.org/10.1016/j.apsusc.2014.12.090>
- Bonilla-Petriciolet A, Mendoza-Castillo DI, Reynel-Ávila HE (2017) Adsorption processes for water treatment and purification. Springer International Publishing, Cham
- Brooker MH, Irish DE (1968) Infrared and Raman spectral studies of KNO<sub>2</sub>–KNO<sub>3</sub> solutions. *Can J Chem* 46:229–233. <https://doi.org/10.1139/v68-036>
- Cardoza LA, Knapp CW, Larive CK, Belden JB, Lydy M, Graham DW (2005) Factors affecting the fate of ciprofloxacin in aquatic field systems. *Water Air Soil Pollut* 161:383–398. <https://doi.org/10.1007/s11270-005-5550-6>
- Chen M, Chu W (2016) H<sub>2</sub>O<sub>2</sub> assisted degradation of antibiotic norfloxacin over simulated solar light mediated Bi<sub>2</sub>WO<sub>6</sub>: Kinetics and reaction pathway. *Chem Eng J* 296:310–318. <https://doi.org/10.1016/j.cej.2016.03.083>
- Chen A-H, Liu S-C, Chen C-Y, Chen C-Y (2008) Comparative adsorption of Cu(II), Zn(II), and Pb(II) ions in aqueous solution on the crosslinked chitosan with epichlorohydrin. *J Hazard Mater* 154:184–191. <https://doi.org/10.1016/j.jhazmat.2007.10.009>
- Chowdhury S, Balasubramanian R (2014) Recent advances in the use of graphene-family nanoadsorbents for removal of toxic pollutants from wastewater. *Adv Colloid Interf Sci* 204:35–56. <https://doi.org/10.1016/j.cis.2013.12.005>
- Cortés-Arriagada D, Toro-Labbé A (2016) Aluminum and iron doped graphene for adsorption of methylated arsenic pollutants. *Appl Surf Sci* 386:84–95. <https://doi.org/10.1016/j.apsusc.2016.05.154>
- Delgado N, Capparelli A, Navarro A, Marino D (2019) Pharmaceutical emerging pollutants removal from water using powdered activated carbon: study of kinetics and adsorption equilibrium. *J Environ Manag* 236:301–308. <https://doi.org/10.1016/j.jenvman.2019.01.116>
- Ding D, Liu C, Ji Y, Yang Q, Chen L, Jiang C, Cai T (2017) Mechanism insight of degradation of norfloxacin by magnetite nanoparticles activated persulfate: identification of radicals and degradation pathway. *Chem Eng J* 308:330–339. <https://doi.org/10.1016/j.cej.2016.09.077>
- Dong L, Chen Z, Zhao X, Ma J, Lin S, Li M, Bao Y, Chu L, Leng K, Lu H, Loh KP (2018) A non-dispersion strategy for large-scale production of ultra-high concentration graphene slurries in water. *Nat Commun* 9:76. <https://doi.org/10.1038/s41467-017-02580-3>
- Doyurum YS, Akyil ES (2011) Sorption behaviors of uranium (VI) ions on  $\alpha$ -FeOOH. *Desalination* 269:58–66. <https://doi.org/10.1016/j.desal.2010.10.042>
- Ebele AJ, Abou-Elwafa Abdallah M, Harrad S (2017) Pharmaceuticals and personal care products (PPCPs) in the freshwater aquatic environment. *Emerg Contam* 3:1–16. <https://doi.org/10.1016/j.emcon.2016.12.004>
- El-Shafai NM, El-Khouly ME, El-Kemary M et al (2019) Fabrication and characterization of graphene oxide–titanium dioxide nanocomposite for degradation of some toxic insecticides. *J Ind Eng Chem* 69:315–323. <https://doi.org/10.1016/j.jiec.2018.09.045>
- Feng Z, Odelius K, Rajarao GK, Hakkarainen M (2018) Microwave carbonized cellulose for trace pharmaceutical adsorption. *Chem Eng J* 346:557–566. <https://doi.org/10.1016/j.cej.2018.04.014>
- Foureaux AFS, Reis EO, Lebron Y, Moreira V, Santos LV, Amaral MS, Lange LC (2019) Rejection of pharmaceutical compounds from surface water by nanofiltration and reverse osmosis. *Sep Purif Technol* 212:171–179. <https://doi.org/10.1016/j.seppur.2018.11.018>
- Ganguly A, Sharma S, Papakonstantinou P, Hamilton J (2011) Probing the thermal deoxygenation of graphene oxide using high-resolution in situ X-ray-based spectroscopies. *J Phys Chem C* 115:17009–17019. <https://doi.org/10.1021/jp203741y>
- Gao Y, Li Y, Zhang L, Huang H, Hu J, Shah SM, Su X (2012) Adsorption and removal of tetracycline antibiotics from aqueous solution by graphene oxide. *J Colloid Interface Sci* 368:540–546. <https://doi.org/10.1016/j.jcis.2011.11.015>
- Gomes J, Costa R, Quinta-Ferreira RM, Martins RC (2017) Application of ozonation for pharmaceuticals and personal care products removal from water. *Sci Total Environ* 586:265–283. <https://doi.org/10.1016/j.scitotenv.2017.01.216>
- Gou J, Ma Q, Deng X, Cui Y, Zhang H, Cheng X, Li X, Xie M, Cheng Q (2017) Fabrication of Ag<sub>2</sub>O/TiO<sub>2</sub>-zeolite composite and its enhanced solar light photocatalytic performance and mechanism for degradation of norfloxacin. *Chem Eng J* 308:818–826. <https://doi.org/10.1016/j.cej.2016.09.089>
- Gregg SJ, Sing KSW, Salzberg HW (1967) Adsorption surface area and porosity. *J Electrochem Soc* 114:279C. <https://doi.org/10.1149/1.2426447>
- Guźda B, Buchwald T, Nocuń M, Bąkiewicz A, Krawczyk P (2017) Graphene material preparation through thermal treatment of graphite oxide electrochemically synthesized in aqueous sulfuric acid. *RSC Adv* 7:19904–19911. <https://doi.org/10.1039/c7ra01678f>
- Ikehata K, Jodeiri Naghashkar N, Gamal El-Din M (2006) Degradation of aqueous pharmaceuticals by ozonation and advanced oxidation processes: a review. *Ozone Sci Eng* 28:353–414. <https://doi.org/10.1080/01919510600985937>
- Inglezakis VJ, Pouloupoulos SG, Kazemian H (2018) Insights into the S-shaped sorption isotherms and their dimensionless forms.

- Microporous Mesoporous Mater 272:166–176. <https://doi.org/10.1016/j.micromeso.2018.06.026>
- Jiang LH, Guo LY, Ming ZG et al (2016) Removal of 17 $\beta$ -estradiol by few-layered graphene oxide nanosheets from aqueous solutions: external influence and adsorption mechanism. *Chem Eng J* 284:93–102. <https://doi.org/10.1016/j.cej.2015.08.139>
- Kim H, Kang S-O, Park S, Park HS (2015) Adsorption isotherms and kinetics of cationic and anionic dyes on three-dimensional reduced graphene oxide macrostructure. *J Ind Eng Chem* 21:1191–1196. <https://doi.org/10.1016/j.jiec.2014.05.033>
- Kleiser G, Frimmel FH (2000) Removal of precursors for disinfection by-products (DBPs) — differences between ozone- and OH-radical-induced oxidation. *Sci Total Environ* 256:1–9. [https://doi.org/10.1016/S0048-9697\(00\)00377-6](https://doi.org/10.1016/S0048-9697(00)00377-6)
- Konicki W, Aleksandrak M, Moszyński D, Mijowska E (2017) Adsorption of anionic azo-dyes from aqueous solutions onto graphene oxide: equilibrium, kinetic and thermodynamic studies. *J Colloid Interface Sci* 496:188–200. <https://doi.org/10.1016/j.jcis.2017.02.031>
- Lebron YAR, Moreira VR, Santos LVS, Jacob RS (2018) Remediation of methylene blue from aqueous solution by *Chlorella pyrenoidosa* and *Spirulina maxima* biosorption: equilibrium, kinetics, thermodynamics and optimization studies. *J Environ Chem Eng* 6:6680–6690. <https://doi.org/10.1016/j.jece.2018.10.025>
- Lebron YAR, Moreira VR, Santos LVS (2019) Studies on dye biosorption enhancement by chemically modified *Fucus vesiculosus*, *Spirulina maxima* and *Chlorella pyrenoidosa* algae. *J Clean Prod* 240:118197. <https://doi.org/10.1016/j.jclepro.2019.118197>
- Ma X, Cheng Y, Ge Y, Wu H, Li Q, Gao N, Deng J (2018) Ultrasound-enhanced nanosized zero-valent copper activation of hydrogen peroxide for the degradation of norfloxacin. *Ultrason Sonochem* 40:763–772. <https://doi.org/10.1016/j.ultsonch.2017.08.025>
- Madarang CJ, Kim HY, Gao G, Wang N, Zhu J, Feng H, Goring M, Kasner ML, Hou S (2012) Adsorption behavior of EDTA-Graphene oxide for Pb (II) removal. *ACS Appl Mater Interfaces* 4:1186–1193. <https://doi.org/10.1021/am201645g>
- Marcano DC, Kosynkin DV, Berlin JM, Sinitkii A, Sun Z, Slesarev A, Alemany LB, Lu W, Tour JM (2010) Improved synthesis of graphene oxide. *ACS Nano* 4:4806–4814. <https://doi.org/10.1021/nl1006368>
- Marcelino RBP, Andrade LN, Starling MCV, Amorim CC, Barbosa MLT, Lopes RP, Reis BG, Leão MMD (2016) Evaluation of aerobic and anaerobic biodegradability and toxicity assessment of real pharmaceutical wastewater from industrial production of antibiotics. *Brazilian J Chem Eng* 33:445–452. <https://doi.org/10.1590/0104-6632.20160333s20150136>
- Martins M, Sanches S, Pereira IAC (2018) Anaerobic biodegradation of pharmaceutical compounds: new insights into the pharmaceutical-degrading bacteria. *J Hazard Mater* 357:289–297. <https://doi.org/10.1016/j.jhazmat.2018.06.001>
- Moreira VR, Lebron YAR, Freire SJ, Santos LVS, Palladino F, Jacob RS (2019) Biosorption of copper ions from aqueous solution using *Chlorella pyrenoidosa*: optimization, equilibrium and kinetics studies. *Microchem J* 145:119–129. <https://doi.org/10.1016/j.microc.2018.10.027>
- Nachiappan S, Senthil Kumar P, Gopinath KP, Rajinikanth V, Baskaran R, Babu Ponnusami A (2018) Intensified degradation of pharmaceutical effluents by novel aerobic iron-swarf activated molecular oxygen in the presence of ascorbic acid. *Desalin Water Treat* 102:273–279. <https://doi.org/10.5004/dwt.2018.21846>
- Nariyan E, Aghababaei A, Sillanpää M (2017) Removal of pharmaceutical from water with an electrocoagulation process: effect of various parameters and studies of isotherm and kinetic. *Sep Purif Technol* 188:266–281. <https://doi.org/10.1016/j.seppur.2017.07.031>
- Nascimento RF, Lima ACA, Vidal CB, et al (2014) Adsorção: Aspectos teóricos e aplicações ambientais
- Ola S, Erland B (2015) Thermal stability assessment of antibiotics in moderate temperature and subcritical water using a pressurized dynamic flow-through system. *Int J Innov Appl Stud* 11:872–880
- Pang X, Ran X, Kuang F et al (2010) Inhibiting effect of ciprofloxacin, norfloxacin and ofloxacin on corrosion of mild steel in hydrochloric acid. *Chinese J Chem Eng* 18:337–345. [https://doi.org/10.1016/S1004-9541\(08\)60362-6](https://doi.org/10.1016/S1004-9541(08)60362-6)
- Pavithra KG, Senthil Kumar P, Sundar Rajan P, Saravanan A, Naushad M (2017) Sources and impacts of pharmaceutical components in wastewater and its treatment process: a review. *Korean J Chem Eng* 34:2787–2805. <https://doi.org/10.1007/s11814-017-0255-2>
- Peng G, Zhang M, Deng S, Shan D, He Q, Yu G (2018) Adsorption and catalytic oxidation of pharmaceuticals by nitrogen-doped reduced graphene oxide/Fe<sub>3</sub>O<sub>4</sub> nanocomposite. *Chem Eng J* 341:361–370. <https://doi.org/10.1016/j.cej.2018.02.064>
- Pereira AMPT, Silva LJJ, Meisel LM, Pena A (2015) Fluoroquinolones and tetracycline antibiotics in a Portuguese aquaculture system and aquatic surroundings: occurrence and environmental impact. *J Toxicol Environ Heal - Part A Curr Issues* 78:959–975. <https://doi.org/10.1080/15287394.2015.1036185>
- Polishchuk AV, Karaseva ÉT, Emelina TB, Nikolenko YM, Karasev VE (2009) Electronic structure and spectroscopic properties of norfloxacin, enoxacin, and nalidixic acid. *J Struct Chem* 50:434–438. <https://doi.org/10.1007/s10947-009-0065-4>
- Pouretedal HR, Sadegh N (2014) Effective removal of amoxicillin, cephalexin, tetracycline and penicillin G from aqueous solutions using activated carbon nanoparticles prepared from vine wood. *J Water Process Eng* 1:64–73. <https://doi.org/10.1016/j.jwpe.2014.03.006>
- Prabavathi SL, Govindan K, Saravanakumar K, Jang A, Muthuraj V (2019) Construction of heterostructure CoWO<sub>4</sub>/g-C<sub>3</sub>N<sub>4</sub> nanocomposite as an efficient visible-light photocatalyst for norfloxacin degradation. *J Ind Eng Chem* 80:558–567. <https://doi.org/10.1016/j.jiec.2019.08.035>
- Prasannamedha G, Kumar PS (2020) A review on contamination and removal of sulfamethoxazole from aqueous solution using cleaner techniques: present and future perspective. *J Clean Prod* 250:119553. <https://doi.org/10.1016/j.jclepro.2019.119553>
- Pruthiwanasan B, Phechkrajang C, Sumtornsuk L (2016) Fluorescent labelling of ciprofloxacin and norfloxacin and its application for residues analysis in surface water. *Talanta* 159:74–79. <https://doi.org/10.1016/j.talanta.2016.05.080>
- Rana RS, Singh P, Kandari V, Singh R, Dobhal R, Gupta S (2017) A review on characterization and bioremediation of pharmaceutical industries' wastewater: an Indian perspective. *Appl Water Sci* 7:1–12. <https://doi.org/10.1007/s13201-014-0225-3>
- Reis EO, Foureaux AFS, Rodrigues JS, Moreira VR, Lebron YAR, Santos LVS, Amaral MCS, Lange LC (2019) Occurrence, removal and seasonal variation of pharmaceuticals in Brazilian drinking water treatment plants. *Environ Pollut* 250:773–781. <https://doi.org/10.1016/j.envpol.2019.04.102>
- Renita AA, Kumar PS, Srinivas S et al (2017) A review on analytical methods and treatment techniques of pharmaceutical wastewater. *Desalin Water Treat* 87:160–178. <https://doi.org/10.5004/dwt.2017.21311>
- Rostamian R, Behnejad H (2016) A comparative adsorption study of sulfamethoxazole onto graphene and graphene oxide nanosheets through equilibrium, kinetic and thermodynamic modeling. *Process Saf Environ Prot* 102:20–29. <https://doi.org/10.1016/j.psep.2015.12.011>
- Rostvall A, Zhang W, Dürig W, Renman G, Wiberg K, Ahrens L, Gago-Ferrero P (2018) Removal of pharmaceuticals, perfluoroalkyl substances and other micropollutants from wastewater using lignite, Xylit, sand, granular activated carbon (GAC) and GAC+Polonite®

- in column tests – role of physicochemical properties. *Water Res* 137: 97–106. <https://doi.org/10.1016/j.watres.2018.03.008>
- Sahoo S, Chakraborti CK, Behera PK, Mishra SC (2012) FTIR and Raman spectroscopic investigations of a Norfloxacin/Carbopol934 polymeric suspension. *J Young Pharm* 4:138–145. <https://doi.org/10.4103/0975-1483.100017>
- Samiee R, Ramezanzadeh B, Mahdavian M, Alibakhshi E, Bahlakeh G (2019) Graphene oxide nano-sheets loading with praseodymium cations: adsorption-desorption study, quantum mechanics calculations and dual active-barrier effect for smart coatings fabrication. *J Ind Eng Chem* 78:143–154. <https://doi.org/10.1016/j.jiec.2019.06.024>
- Santos LV d S, Meireles AM, Lange LC (2015) Degradation of antibiotics norfloxacin by Fenton, UV and UV/H<sub>2</sub>O<sub>2</sub>. *J Environ Manag* 154:8–12. <https://doi.org/10.1016/j.jenvman.2015.02.021>
- Sayed M, Khan JA, Shah LA, Shah NS, Khan HM, Rehman F, Khan AR, Khan AM (2016) Degradation of quinolone antibiotic, norfloxacin, in aqueous solution using gamma-ray irradiation. *Environ Sci Pollut Res* 23:13155–13168. <https://doi.org/10.1007/s11356-016-6475-x>
- Senthil Kumar P, Saravanan A (2018) A biological approach for the removal of pharmaceutical pollutants from wastewater. In: *Life Cycle Assessment of Wastewater Treatment*. CRC Press, pp 117–137
- Senthil Kumar P, Saravanan A (2019) New analytical approaches for pharmaceutical wastewater treatment using graphene based materials. In: *A new generation material graphene: applications in water technology*. Springer International Publishing, Cham, pp 397–411
- Shen Y, Zhu C, Song S, Zeng T, Li L, Cai Z (2019) Defect-abundant covalent Triazine frameworks as sunlight-driven self-cleaning adsorbents for volatile aromatic pollutants in water. *Environ Sci Technol* 53:9091–9101. <https://doi.org/10.1021/acs.est.9b02222>
- Sheng G, Huang C, Chen G, Sheng J, Ren X, Hu B, Ma J, Wang X, Huang Y, Alsaedi A, Hayat T (2018) Adsorption and co-adsorption of graphene oxide and Ni(II) on iron oxides: a spectroscopic and microscopic investigation. *Environ Pollut* 233:125–131. <https://doi.org/10.1016/j.envpol.2017.10.047>
- Shi Y, Chen S, Ma M, Wu B, Ying J, Xu X, Wang X (2016) Highly efficient and antibacterial zinc norfloxacin thermal stabilizer for poly(vinyl chloride). *RSC Adv* 6:97491–97502. <https://doi.org/10.1039/C6RA17912F>
- Stafford J, Patapas A, Uzo N, Matar OK, Petit C (2018) Towards scale-up of graphene production via nonoxidizing liquid exfoliation methods. *AIChE J* 64:3246–3276. <https://doi.org/10.1002/aic.16174>
- Tang Y, Guo H, Xiao L, Yu S, Gao N, Wang Y (2013) Synthesis of reduced graphene oxide/magnetite composites and investigation of their adsorption performance of fluoroquinolone antibiotics. *Colloids Surfaces A Physicochem Eng Asp* 424:74–80. <https://doi.org/10.1016/j.colsurfa.2013.02.030>
- Thommes M, Kaneko K, Neimark AV, Olivier JP, Rodriguez-Reinoso F, Rouquerol J, Sing KSW (2015) Physisorption of gases, with special reference to the evaluation of surface area and pore size distribution (IUPAC technical report). *Pure Appl Chem* 87:1051–1069. <https://doi.org/10.1515/pac-2014-1117>
- Van Doorslaer X, Dewulf J, Van Langenhove H, Demeestere K (2014) Fluoroquinolone antibiotics: an emerging class of environmental micropollutants. *Sci Total Environ* 500–501:250–269. <https://doi.org/10.1016/j.scitotenv.2014.08.075>
- Viana MM, Lima MCFS, Forsythe JC, Gangoli VS, Cho M, Cheng Y, Silva GG, Wong MS, Caliman V (2015) Facile graphene oxide preparation by microwave-assisted acid method. *J Braz Chem Soc* 26:978–984. <https://doi.org/10.5935/0103-5053.20150061>
- Voylov D, Saito T, Lokitz B, Uhrig D, Wang Y, Agapov A, Holt A, Bocharova V, Kisliuk A, Sokolov AP (2016) Graphene oxide as a radical initiator: free radical and controlled radical polymerization of sodium 4-vinylbenzenesulfonate with graphene oxide. *ACS Macro Lett* 5:199–202. <https://doi.org/10.1021/acsmacrolett.6b00003>
- Wang J, Chen B (2015) Adsorption and coadsorption of organic pollutants and a heavy metal by graphene oxide and reduced graphene materials. *Chem Eng J* 281:379–388. <https://doi.org/10.1016/j.cej.2015.06.102>
- Yang W, Lu Y, Zheng F, Xue X, Li N, Liu D (2012) Adsorption behavior and mechanisms of norfloxacin onto porous resins and carbon nanotube. *Chem Eng J* 179:112–118. <https://doi.org/10.1016/j.cej.2011.10.068>
- Yu H, Zhang B, Bulin C, Li R, Xing R (2016) High-efficient synthesis of graphene oxide based on improved hummers method. *Sci Rep* 6: 36143. <https://doi.org/10.1038/srep36143>
- Zhang Y, Cheng Y, Chen N, Zhou Y, Li B, Gu W, Shi X, Xian Y (2014) Recyclable removal of bisphenol a from aqueous solution by reduced graphene oxide–magnetic nanoparticles: adsorption and desorption. *J Colloid Interface Sci* 421:85–92. <https://doi.org/10.1016/j.jcis.2014.01.022>
- Zhang Q, Zhang S-H, Wang Z, Guo M, Liu JN, Shi LL, Gu W (2017) Pollution level, distribution characteristics and risk assessment of 32 PPCPs in surface water of Luomahu Lake. *Huan jing ke xue = Huanjing kexue* 38:162–169. <https://doi.org/10.13227/j.hjkk.201606184>
- Zhang Y, Li H, Huang H, Zhang Q, Guo Q (2018) Graphene oxide–supported cobalt phthalocyanine as heterogeneous catalyst to activate peroxymonosulfate for efficient degradation of norfloxacin antibiotics. *J Environ Eng* 144:04018052. [https://doi.org/10.1061/\(ASCE\)EE.1943-7870.0001395](https://doi.org/10.1061/(ASCE)EE.1943-7870.0001395)

**Publisher's note** Springer Nature remains neutral with regard to jurisdictional claims in published maps and institutional affiliations.